

Layton: Latent Consistency Tokenizer for 1024-pixel Image Reconstruction and Generation by 256 Tokens

Qingsong Xie
OPPO AI Center

xieqingsong1@oppo.com

Zhao Zhang
ByteDance

zzhang@mail.nankai.edu.cn

Zhe Huang
Tsinghua University

huangz23@mails.tsinghua.edu.cn

Yanhao Zhang
OPPO AI Center

zhangyanhao@oppo.com

Haonan Lu
OPPO AI Center

luhaonan@oppo.com

Zhenyu Yang
OPPO AI Center

yangzhenyu@oppo.com



Figure 1: 1024-pixel image generation results of LaytonGen-T* in an autoregressive way with **256 tokens**, demonstrating the capability of LaytonGen-T* in high-quality image synthesis.

Abstract

Image tokenization has significantly advanced visual generation and multimodal modeling, particularly when paired with autoregressive models. However, current methods face challenges in balancing efficiency and fidelity: high-resolution image reconstruction either requires an excessive number of tokens or compromises critical details through token reduction. To resolve this, we propose Latent Consistency Tokenizer (Layton) that bridges discrete visual

tokens with the compact latent space of pre-trained Latent Diffusion Models (LDMs), enabling efficient representation of 1024×1024 images using only 256 tokens—a $16\times$ compression over VQGAN. Layton integrates a transformer encoder, a quantized codebook, and a latent consistency decoder (LCD). Direct application of LDM as the decoder results in color and brightness discrepancies; thus, we convert it to latent consistency decoder, reducing multi-step sampling to 1-2 steps for direct pixel-level supervision. Experiments demonstrate Layton’s superiority in high-fidelity

reconstruction, with 10.8 reconstruction Frechet Inception Distance on MSCOCO-2017 5K benchmark for 1024×1024 image reconstruction. We also extend Layton to a text-to-image generation model, LaytonGen, working in autoregression. It achieves 0.73 score on GenEval benchmark, surpassing current state-of-the-art methods. The code and model will be released.

1. Introduction

Image tokenizer [38, 48] aims to convert images from their raw pixel-based representations into discrete visual tokens, which can then be used to reconstruct the original image through its corresponding decoder. This approach has garnered significant attention due to its crucial role in image generation, particularly in autoregressive models [33, 37, 40] and masked transformers [1, 2, 4, 43].

A representative approach, VQGAN [46] learns a codebook to quantize continuous embeddings of a 256×256 image into 256 discrete tokens using a spatial downsampling ratio of $16 \times$ —a standard configuration in recent works [24, 27, 32, 33]. When it comes to high-resolution image reconstruction or generation, e.g., 1024×1024 pixels, requires predicting 4096 tokens, creating substantial challenges in both computational efficiency and model optimization. This lengthy token sequence complicates downstream applications, such as integrating visual tokens into large multi-modal models for interleaved text and image understanding and generation. While recent advancements explore token compression through residual codebooks [16, 37] and 1D tokenization [13, 48] for 256×256 images, these approaches have not substantially addressed the challenges of higher-resolution image reconstruction and generation. Recent latent diffusion models (LDMs) [5, 15, 26] have demonstrated remarkable success in 1024×1024 image generation by operating in low-dimensional latent spaces. This raises a compelling question: Can discrete visual tokens be aligned with the compact latent space of LDMs to leverage their powerful decoders for high-fidelity reconstruction and generation use?

In this paper, we introduce a Latent Consistency Tokenizer (Layton), comprising a transformer encoder, a quantized vector codebook, and a latent consistency decoder. Our key insight is to align discrete visual tokens with the compact latent space of pre-trained LDMs, enabling efficient representation of 1024×1024 images with only 256 tokens—a $16 \times$ reduction compared to VQGAN. Inspired by ControlNet [50], we first employ a latent diffusion decoder through copying adaptive blocks in LDM with zero convolution connecting copy and raw LDM. During training, Layton is optimized using diffusion objectives with progressive resolution scaling from 512×512 to 1024×1024 . However, relying solely on diffusion loss re-

sults in reconstructed images with noticeable discrepancies in color and brightness. To address this, we introduce latent consistency models [28, 44] to the decoder, converting the multi-step sampling process into one or two steps. It enables more direct supervision and improving reconstruction fidelity. Moreover, we extend Layton to text-to-image generation model (LaytonGen) by training an autoregressive transformer, which efficiently generates these compact token sequences through text-instructed autoregressive prediction.

We conducted comprehensive experiments to evaluate Layton on the ImageNet 50K [3], MSCOCO-2017 5K [21] benchmarks. With 256 tokens to reconstruct 1024×1024 pixel images, Layton achieves 10.80 reconstruction Frechet Inception Distance (rFID) score [9] on MSCOCO-2017, significantly outperforming VQGAN [46], TiTok [48], LlamaGen [33]. On ImageNet benchmark, Layton gets 2.78 rFID, surpassing VQGAN and LlamaGen, comparable to TiTok, but with much better Peak Signal-to-Noise Ratio, Structural Similarity Index Measure, and Learned Perceptual Image Patch Similarity than TiTok. For text-to-image task, LaytonGen obtains 0.73 score on GenEval benchmark [8], superior to other diffusion and autoregressive models, e.g., 0.62 by SD3 [6], 0.56 by HART [34], 0.53 by Show-o [43], and 0.32 by LlamaGen.

Our contributions are threefold:

- We propose Layton, an image tokenizer that bridges discrete visual tokens with the latent space of pre-trained LDMs, demonstrating the ability to reconstruct and generate 1024×1024 images with only 256 tokens.
- To alleviate color and brightness discrepancies caused by diffusion objective in reconstruction, we integrate latent consistency model into latent diffusion decoder with direct pixel-level supervision through efficient few-step sampling.
- Built on Layton, LaytonGen can generate high-quality 1024×1024 images via text-guided autoregressive token prediction. It achieves leading performances on multiple synthesis benchmarks.

2. Related Work

2.1. Image Tokenization

Variational Autoencoders (VAEs) [14] represent a significant advancement in the field by learning to map inputs to a distribution. Building upon this foundation, VQ-VAEs [38] learn discrete representations that form a categorical distribution. This process is further improved in VQGAN [7], which enhances the training process through the integration of adversarial training techniques. The transformer architecture within autoencoders is explored in ViT-

VQGAN [46]. RQ-VAE [16], introduces residual quantization to the VAE framework, recursively quantizes the feature map in a coarse-to-fine manner, allowing for a precise approximation of the feature map with a fixed codebook size. In a different vein, MAGVIT-v2 [47], FSQ [23], BSQ-ViT [53] propose lookup-free quantization, presenting an alternative approach that bypasses traditional lookup mechanisms. TiTok [48] performs 2D-to-1D distillation, compressing the number of tokens used to represent the same image. VILA-U [42], TokenFlow [27], and TA-TiTok [13] introduce text supervision to enhance semantic information for discrete tokens. DiVAE [32] introduces a diffusion decoder, turning single-step decoding into a multistep probabilistic process at the pixel level. However, they can not reconstruct or generate high-resolution image details by small number of tokens. Motivated by LDMs [6, 15, 26] which are able to generate high-resolution, high-quality images, we explore effective method to leverage the pre-trained LDM as decoder to reconstruct high-resolution images.

2.2. Tokenized Image Generation

Image tokenization has become a powerful technique for image generation, allowing images to be represented as discrete tokens that can be manipulated and generated using various modeling approaches. Two prominent methodologies in this domain are the masked-transformer style and the autoregressive style. In the masked-transformer style, methods like MaskGIT [2] employ a bidirectional transformer decoder. During training, the model predicts randomly masked tokens and iteratively refines the image at inference. Other notable works in this category include [1, 17, 18, 19]. Conversely, the autoregressive style involves predicting all tokens of an image in a serialized manner, akin to next-word prediction [7, 22]. This approach naturally integrates with the multimodal large language model [12, 36, 42, 49] and is conducive to unifying various modalities. LlamaGen [33] stands out as a simple yet effective generation method that adopts the autoregressive approach, but it fails to generate satisfactory images. We extend Layton to conditional generation model by training an autoregressive model to predict the next discrete tokens produced by the tokenizer. Thanks to the excellent performance of Layton to reconstruct images, our model is able to generate superior images.

3. Preliminary

3.1. VQGAN.

VQGAN [7] typically consists of encoder Enc , quantizer Q , and decoder Dec . Given an image $\mathbf{x} \in \mathbb{R}^{H \times W \times 3}$, where H, W denotes image height and width, respectively, Enc firsts extracts its latent embeddings $\mathbf{G} = Enc(\mathbf{x}) \in \mathbb{R}^{H/f \times W/f \times D}$, effectively reducing the spatial dimensions by a factor of f . Then, Q maps each embedding $\mathbf{g} \in \mathbb{R}^D$ in

\mathbf{G} with D representing embedding dimension to the nearest code c_i in a learnable codebook $\mathbb{C} \in \mathbb{R}^{N \times D}$, where N is the codebook size. Mathematically, this can be formulated as:

$$Q(\mathbf{g}) = \mathbf{c}_{Tok}, \quad Tok = \arg \min_{j \in \{1, 2, \dots, N\}} \|\mathbf{g} - \mathbf{c}_j\|_2^2. \quad (1)$$

The mapped feature vectors $\mathbf{C} \in \mathbb{R}^{H/f \times W/f \times D}$ are calculated by $Q(\mathbf{G})$, while decoder converts \mathbf{C} to image $\hat{\mathbf{x}}$ through $Dec(\mathbf{C})$.

3.2. Diffusion Models.

Diffusion model [10] is composed of a forward diffusion process and a reverse denoising process. Forward process gradually adds random noise to clean data \mathbf{x}_0 and diffuses it into pure Gaussian noise as:

$$\mathbf{x}_t = \alpha_t \mathbf{x}_0 + \beta_t \epsilon, \quad t \in [0, T], \quad (2)$$

where $\epsilon \in \mathcal{N}(0, \mathbf{I})$, α_t, β_t are scheduler coefficients with $\alpha_t^2 + \beta_t^2 = 1$, and T is the ending time. During the training stage, DMs usually minimizes diffusion loss \mathcal{L}_{DF} via neural network ϵ_θ predicting noise as:

$$\mathcal{L}_{DF} = \|\epsilon_\theta(\mathbf{x}_t, t) - \epsilon\|_2^2. \quad (3)$$

Denoising process reverses the diffusion process to create clean samples from the Gaussian noise.

To reduce resource consumption, Latent Diffusion Models (LDMs) [5, 15, 26] transform pixel image \mathbf{x}_0 into latent embedding \mathbf{z}_0 via VAE, and perform diffusion and denoising operations in latent space. Sequentially, VAE decoder converts predicted \mathbf{z}_0 back to the pixel image. LDMs has shown great success in text-to-image, image-to-image tasks, but they have not been explored for building discrete tokenizer. In this study, we investigate effective method which enables LDMs to construct discrete tokenizer for high-resolution image reconstruction and generation.

4. Methodology

Conventional discrete tokenizers [7, 33, 38, 46, 48] encode images into discrete tokens and decode the tokens into original images in pixel space. These works transform text-to-image generation into next-prediction task, which predict image tokens by autoregressive model conditioned on the text input. However, these tokenizers need a large number of tokens to generate high-resolution images, leading to prohibitive training and inference costs. Moreover, these tokenizers can not faithfully reconstruct images with intricate, high-frequency details such as human faces. Such drawback sets a low ceiling for text-to-image generation task.

As a result, we are targeting at constructing an innovative tokenizer for high-resolution image reconstruction and generation via a small number of discrete tokens. To this end,

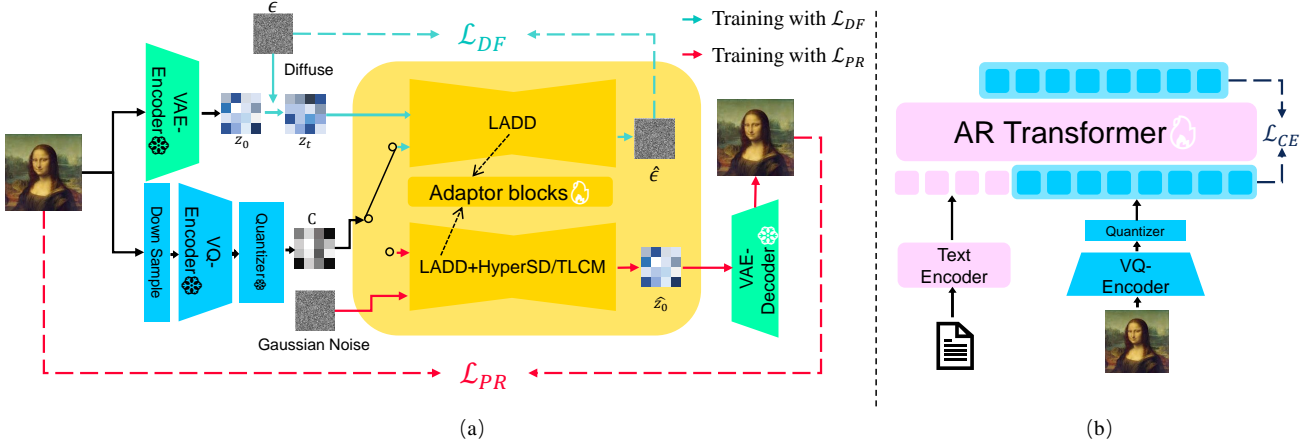


Figure 2: (a) Overview of Layton. The input image is sequentially processed by downsampler, encoder and quantizer into condition features. It also goes through the VAE Encoder in pretrained LDM to produce latent z_0 , which will be diffused to produce z_t . LADD takes C , z_t and t as input. In the first phase, we apply \mathcal{L}_{DF} to train LADD. In the second phase, we introduce acceleration models to LADD and replace z_t with Gaussian noise to perform one or two step inference, which allows us to train LADD with pixel reconstruction loss \mathcal{L}_{PR} . For simplicity, we omit the time step t . (b) Illustration of autoregressive text-to-image generation with LaytonGen.

we propose Latent Consistency Tokenizer (Layton) which is capable of reconstructing and producing high-quality images with only 256 tokens. Unlike the existing tokenizers that operate image encoding and decoding in pixel space, Layton models decoding procedure in latent space through unleashing the potential of latent diffusion model, which further makes use of latent consistency models [28, 44], to enforce pixel reconstruction. Upon Layton, we build an autoregressive model for high-resolution image generation driven by text conditions. Fig. 2 illustrates the overview of the proposed method.

4.1. Latent Diffusion Reconstruction

Considering that latent diffusion models [6, 26] are powerful to synthesize high-quality images, we propose latent diffusion decoder (LADD), denoted as f_θ , to build discrete tokenizer. The core thought of LADD is to predict the latent representation z_0 conditioned on the pixel image x_0 . To fulfill this idea, the raw image $x_0 \in \mathbb{R}^{H \times W \times 3}$ is converted into latent code $z_0 \in \mathbb{R}^{H/8 \times W/8 \times C}$ using VAE encoder of pre-trained LDM, where $H = W \in \{512, 1024\}$. To predict z_0 , diffusion loss is used to train LADD as:

$$\mathcal{L}_{DF} = \|f_\theta(z_t, C, t) - \epsilon\|_2^2, \quad (4)$$

where z_t is obtained by forward diffusion procedure using Eq. (2) in latent space. The condition C is obtained by sequentially encoding x_0 using Enc and the quantizer Q through the Eq. (1). To reduce token number, x_0 is first downsampled into the resolution of $H' \times W'$, where $H' = W' \in \{224, 256, 288\}$. To promote training's stability, we draw inspiration from ControlNet [50] to design

LADD structure. Specifically, LADD freezes the parameters of pre-trained LDM and simultaneously clones some blocks of the LDM to a trainable copy. Zero convolution (ZC) is utilized to connect trainable copy and raw LDM. The output O of LADD block at timestep t is computed as:

$$O = ZC(F_{train}(z_t, C, t)) + F(z_t, t), \quad (5)$$

where F and F_{train} denote the frozen LDM block and trainable block in trainable copy, respectively.

To train our tokenizer and save training resource, the visual encoder and quantizer are initialized using pre-trained LlamaGen tokenizer. Next, we freeze the visual encoder and quantizer, enabling only LADD to undergo training.

4.2. Pixel Reconstruction

The diffusion loss enables the decoder to reconstruct the original image through multi-step sampling. However, we have empirically observed that the reconstructed images exhibit discrepancies in color and brightness compared to the original images. To address this issue, we introduce a pixel reconstruction loss \mathcal{L}_{PR} that compels the decoded image to recover the original image. Since diffusion model requires multi-step sampling to generate images, it is unable to directly minimize \mathcal{L}_{PR} , which consumes a significant amount of GPU memory and may lead to gradient explosion. Consistency model (CM) can enable LDMs to generate images with few-step inference. Therefore, we leverage CM to assist LADD in achieving rapid image reconstruction. As Hyper-SD [28] and Training-efficient Latent Consistency Model (TLCM) [44] show state-of-the-art performance, both of which are CMs for LDM acceleration, they

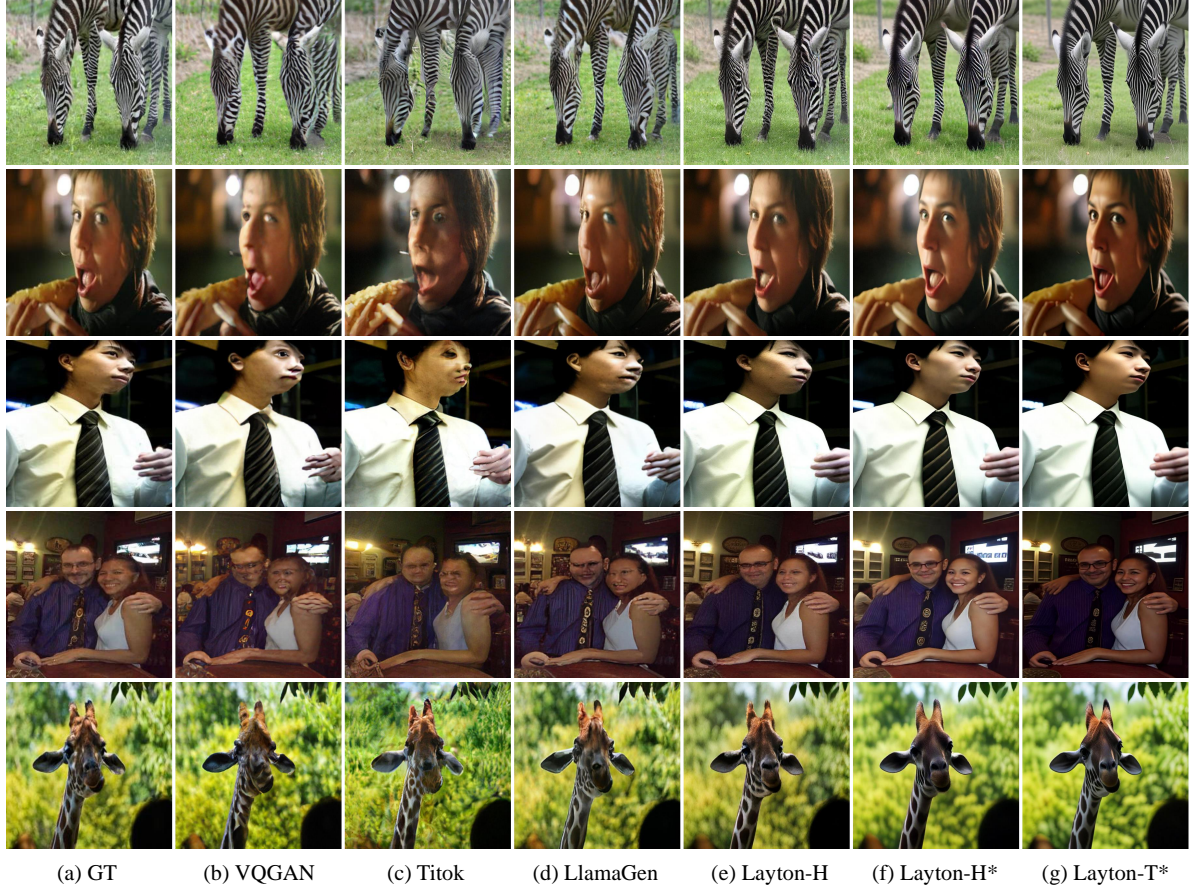


Figure 3: Visual comparisons of images reconstruction for different methods. Layton can achieve much better reconstruction results than VQGAN, TiTok, and LlamaGen, especially in facial reconstruction. The images reconstructed by Layton-H* and Layton-T* show higher quality than other methods, even surpass ground truth (GT).

are integrated into LADD to reconstruct image with few steps. Sequentially, \mathcal{L}_{PR} can be used to optimize our tokenizer as gradient is easily propagated into decoder. One-step sampling is used to reconstruct clean latent code $\hat{\mathbf{z}}_0$ when HyperSD is merged into LADD, because it can generate high-quality image with one step. Two-step sampling is leveraged to restore $\hat{\mathbf{z}}_0$ when incorporating TLCM into LADD since it needs at least two steps, where stop-gradient operation is adopted for the first iteration. Both models accept pure Gaussian noise as initial latent code. The reconstruction loss \mathcal{L}_{PR} is:

$$\mathcal{L}_{PR} = \mathcal{L}_P(\text{Dec}(\hat{\mathbf{z}}_0), \mathbf{x}_0) \quad (6)$$

where $\text{Dec}(\cdot)$ represents the pre-trained VAE decoder in LDM, \mathcal{L}_P is a perceptual loss from LPIPS [51]. We use Layton-H and Layton-T to represent that Hyper-SD and TLCM are utilized in LADD to minimize \mathcal{L}_{PR} , respectively.

4.3. Text-to-image Generation

In order to unleash the value of tokenizer, We leverage Layton to build text-to-image generation model (Layton-Gen). LaytonGen is implemented through autoregressive models P_θ with θ denoting parameters. A text encoder is used to extract text feature \mathbf{f}_{text} , which is projected by an additional MLP to match the dimension of autoregressive models. Cross entropy loss \mathcal{L}_{CE} is applied to train autoregressive model as:

$$\mathcal{L}_{CE} = - \sum_{i=1}^L \log P_\theta(\text{Tok}_{i+1} | \text{Tok}_{1:i}, \mathbf{f}_{text}), \quad (7)$$

where L is token number to represent a image. As classifier-free guidance (CFG) [11] is critical to generate high-quality image in LDM, we adopt it in our models. During training, the conditional is randomly replaced by a null unconditional embedding. During inference stage, the logit ℓ_g is computed as $\ell_g = \ell_u + s(\ell_c - \ell_u)$ for every token, where

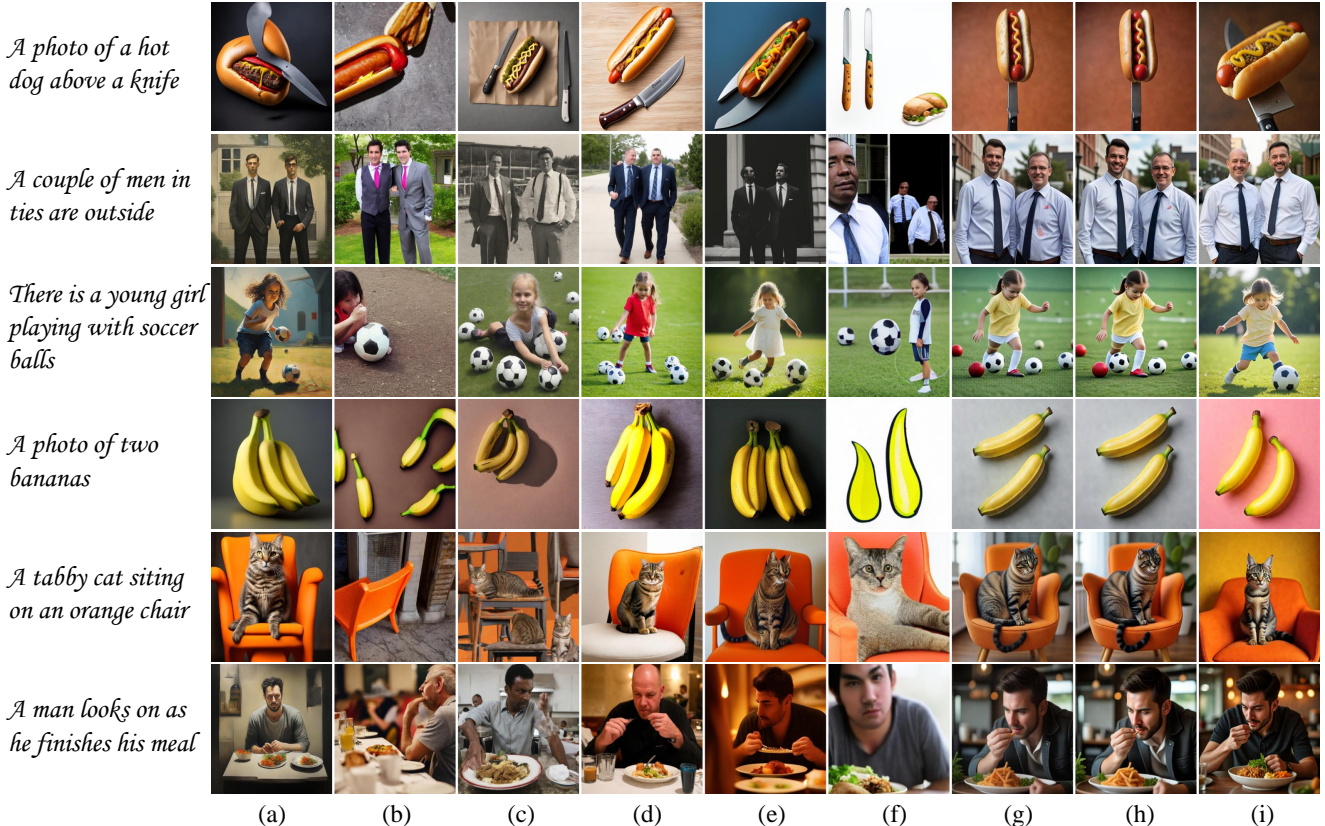


Figure 4: Comparison of text-conditioned generation of different methods. From left to right, (a)HART[35], (b)SD1.5[29], (c)SDXL[26], (d)SD3[5], (e)Show-o[43], (f)LlamaGen[33], (g)LaytonGen-H, (h)LaytonGen-H* and (i)LaytonGen-T*. Apart from satisfactory visual quality, Layton can also yield improved metrics compared to strong baselines.

ℓ_c represents the conditional logit, ℓ_u denotes the unconditional logit, and s is the scaling factor for CFG.

4.4. Data Construction

It is well known that high-quality data is necessary to train LDM, but it is hard to access such real data. To deal with this challenge, we use synthesized data instead of real data to train LaytonGen. After comparing the generated image quality of all open-source models, we select FLUX.1-dev [15] to synthesize data as it presents the highest human preference. The text input for FLUX.1-dev is from LAION-5B [31]. Since raw prompt is too simple to describe image content, we use Qwen2-VL [39] to re-caption the generated images. As Some generated images are not satisfactory, ImageReward (IR) [45] and Multi-dimensional Preference Score (MPS) [52] are used to filter undesirable images, where the images with $IR < 0.8$ or $MPS < 12.0$ are removed. Totally, we synthesize 40M high-quality text-image pairs.

5. Experimental Results

5.1. Image Reconstruction

We employ Peak Signal-to-Noise Ratio (P), Structural Similarity Index Measure (S) to evaluate the image similarity between reconstructed and raw images. Concurrently, we evaluate the distribution discrepancy by reconstruction Frechet Inception Distance score (rFID) [9]. Learned Perceptual Image Patch Similarity (L) [51] is further used to measure perceptual similarity as it performs excellently in terms of human visual perception. The validation is conducted on ImageNet 50K validation set [3], MSCOCO-2017 5K validation set [21], MJHQ-5K validation set which is randomly sampled from MJHQ-30K dataset [25]. All the images are resized to 1024×1024 size for evaluation as we aim at high-resolution image reconstruction.

The performance of different tokenizers is listed in Tab. 1. It can be observed that on ImageNet, TiTok-S-128 [48] gets the slightly lower rFID, but much worse P, S, and L values than Layton-H. This result indicates that compared to Layton-H, the data distribution of images reconstructed by TiTok is closer to that of the original im-

Table 1: The reconstruction performance of Layton on ImageNet, MSCOCO-2017 5K validation dataset, and MJHQ-5K. *Trained on synthesized data by FLux.1-dev.

Methods	#Tokens	ImageNet				MSCOCO-2017				MJHQ-5K			
		rFID↓	P↑	S↑	L↓	rFID↓	P↑	S↑	L↓	rFID↓	P↑	S↑	L↓
VQGAN [7]	256	6.02	19.20	0.60	0.44	14.72	18.78	0.6	0.46	17.58	18.46	0.64	0.45
TiTok-S-128 [48]	128	2.32	16.97	0.51	0.49	12.31	16.47	0.50	0.51	14.17	16.42	0.54	0.50
LlamaGen [33]	256	3.17	19.94	0.64	0.41	11.23	19.53	0.64	0.43	13.26	19.24	0.68	0.41
Layton-H(Ours)	256	2.78	19.80	0.65	0.39	10.80	19.28	0.64	0.41	11.34	19.16	0.68	0.38
Layton-H*(Ours)	256	9.04	19.02	0.65	0.43	16.93	18.20	0.64	0.43	14.02	18.04	0.68	0.39
Layton-T*(Ours)	256	8.71	18.80	0.65	0.43	15.05	17.98	0.64	0.42	13.32	17.81	0.69	0.38

ages. However, the reconstructed images by Layton-H exhibit higher image quality and better structural consistency with the original images, particularly aligning more closely with human visual perception. On MSCOCO-2017 and MJHQ-5K validation sets, Layton-H obtains significant gains than TiTok with respect to all metrics, which demonstrates that Layton-H presents considerably superior generalization performance. We can also find Layton-H outperforms LlamaGen [33] in terms of rFID, S, L metrics, while achieving comparable PSNR value. This is because Layton-H takes advantage of pre-trained LDM assisted by HyperSD to reconstruct images, which is more powerful to restore image details, e.g., human face. Moreover, rFID of Layton-H* and trained on synthesized data is higher than Layton-H and LlamaGen, because data distribution of synthesized data dramatically deviates from those of ImageNet, MSCOCO, and MJHQ sets. The performance of Layton-H* concerning rFID, L are improved by Layton-T*, thanks to its ability to reconstruct intricate, high-frequency by increasing the sampling steps.

Fig. 3 illustrates the visual comparisons of image reconstruction for different tokenizers. We can observe that the proposed Layton-H significantly improves reconstruction performance than VQGAN, TiTok, and LlamaGen, especially in image details such as faces. Besides, it can be seen that the images reconstructed by Layton* and Layton-T* show better quality than other methods, even outperforms ground truth (GT), which implies the potential of our tokenizer to implement super-resolution task. The result also indicates that lower rFID on Imagenet, COCO, MJHQ does not necessarily indicate better reconstruction with respect to human preference.

5.2. Text-to-image Generation

To evaluate the conditional generation performance of Layton, we perform large-scale text-to-image experiments using LaytonGen. The evaluation is conducted on GenEval benchmark [8] and MSCOCO-2017 5K validation dataset [21]. GenEval benchmark is used to evaluate compositional image properties, such as spatial relations

and attribute binding. On MSCOCO dataset, ImageReward (IR), Multi-dimensional Preference Score (MPS), and HPSv2 [41] are used to assess human preference of the generated image, while FaceScore (FS) [20] is adopted to measure image’s face quality.

As listed in Tab. 2, LaytonGen-T* remarkably improves the overall metric of LlamaGen on the GenEval benchmark by 0.41. On MSCOCO-2017 5K validation dataset, LaytonGen-T* again outperforms LlamaGen by a large margin in terms of all metrics. These results indicate that the images generated by LaytonGen-T* significantly outperform those from LlamaGen in terms of overall quality and facial quality. The reason lies in LaytonGen-T*’s ability to fully utilize the generative capabilities of the pre-trained LDM, enabling it to produce intricate, high-frequency details. When compared to SDXL [26], LaytonGen-T* improves the metrics by 0.18 on the Geneval benchmark, while on MSCOCO-2017 dataset, all metrics are enhanced again. One reason behind this is that our Layton-T* can effectively describe intricate, high-resolution images with small number of discrete tokens, allowing LaytonGen-T* to only train an autoregressive model to predict these discrete tokens, which is easier than directly training SDXL through diffusion loss. Another reason is that we have constructed high-quality data to train the autoregressive model. It can also be observed that LaytonGen-T* significantly surpasses other autoregressive models, Show-o and HART on Geneval and MSCOCO-2017 dataset, because they reconstruct images via simple CNN or transformer decoder, failing to reconstruct image details, spatial relations or attribute binding by discrete tokens. Excitingly, on GenEval benchmark, LaytonGen-T* beats SD3 [5] with superior structure MMDiT than UNet in SDXL, and exhibit competitive generation performance on MSCOCO-2017 dataset, which implies that LaytonGen-T maybe improved by adopting SD3 as the decoder. Compared to LaytonGen-H, LaytonGen-H* achieves higher image quality, which results from that the synthesized data facilitates the tokenizer in generating better images. The performance of LaytonGen-H* is further im-

Table 2: The performance of our text-to-image models on GenEval and MSCOCO-2017 5K validation dataset.

Methods	GenEval↑					MSCOCO-2017↑			
	Two Obj	Counting	Position	Color Attri.	Overall	IR	MPS	HPSv2	FS
Diffusion Models									
SD1.5 [29]	0.38	0.35	0.04	0.06	0.43	0.16	10.08	0.285	0.70
SDXL [26]	0.74	0.39	0.15	0.23	0.55	0.82	11.9	0.295	2.94
SD3 [5]	0.74	0.63	0.34	0.36	0.62	1.00	12.59	0.303	3.74
AutoRegressive Models									
LlamaGen [33]	0.34	0.21	0.07	0.04	0.32	0.29	9.56	0.273	0.53
HART [35]	-	-	-	-	0.56	0.66	11.69	0.298	3.50
Show-o [43]	0.52	0.49	0.11	0.28	0.53	0.95	10.58	0.277	2.08
LaytonGen-H	0.67	0.80	0.49	0.50	0.71	0.86	12.22	0.298	2.96
LaytonGen-H*	0.69	0.82	0.51	0.51	0.72	0.88	12.30	0.302	3.20
LaytonGen-T*	0.72	0.84	0.53	0.51	0.73	0.90	12.38	0.304	3.68

Table 3: Ablation study of key components in Layton. VQ-LADD means substituting decoder in LlamaGen with the proposed LADD, and using 25-step DDIM to reconstruct images.

Methods	rFID↓	P↑	S↑	L↓
LlamaGen	13.26	19.24	0.68	0.41
VQ-LADD	12.72	16.53	0.63	0.47
VQ-LADD+Hyper-SD	14.71	16.64	0.64	0.47
VQ-LADD+TLCM	14.40	16.82	0.65	0.45
Layton-H	11.34	19.16	0.68	0.38

Table 4: The effect of token number for Layton-H to reconstruct 1024-pixel image on MJHQ-5K dataset.

#Tokens	rFID↓	P↑	S↑	L↓
192	12.35	18.46	0.66	0.40
256	11.34	19.16	0.68	0.38
324	11.01	19.33	0.69	0.37

proved by LaytonGen-T*, which again verifies that TLCM is more powerful than HyperSD to help decoder generate high-quality images.

As shown in Fig. 4, we can observe that the images generated by LaytonGen-T* enjoy better text-image alignment than other methods, and higher human preference than SD1.5 [30], SDXL, HART [35], Show-o [43], LlamaGen, especially in facial generation.

5.3. Ablation Study

As shown in Tab. 3, we conduct several experiments to verify the effectiveness of the key components with respect to our Layton, where LlamaGen is adopted as baseline.

Latent diffusion decoder. Compared with LLamaGen,

Table 5: The effect of CFG scale for LaytonGen-T* to generate image on MSCOCO-2017 5K validation set.

scale	IR↑	MPS↑	HPSv2↑	FS↑
1.5	0.86	12.37	0.303	3.59
2	0.89	12.38	0.304	3.68
3	0.90	12.40	0.304	3.70
7	0.90	12.41	0.304	3.80

LADD shows worse metrics concerning P, S, L. The reason lies in the fact that LADD predicts the latent representation of the raw image, leading to discrepancies in color and lighting compared to the original image.

LADD acceleration. LADD+Hyper-SD and LADD+TLCM denote that one-step Hyper-SD and three-step TLCM are directly used to accelerate reconstruction procedure. It can be seen that TLCM outperforms Hyper-SD. The probable reason is that TLCM is stronger to reconstruct the fine details of the image due to its better generation performance.

Reconstruction loss. Through optimizing VQ-LADD using pixel reconstruction loss, Layton-H surpasses LLamaGen and VQ-LADD by a large margin in terms of rFID, S, and L metrics. The result indicates that the proposed reconstruction loss is critical to improve tokenizer’s performance, which is able to enforce the reconstructed image close to raw image in pixel space.

Token number. As summarized in Tab. 4, we can see even using 192 tokens, Layton-H can reconstruct 1024-pixel image with high performance. As the increase of the token number, the performance is further improved.

CFG scale. Tab. 5 lists the performance of Layton-T* for text-to-image generation with different CFG scale. It can be observed that Layton-T* is capable of generating

high-quality image using different CFG. The performance can be improved with higher CFG, and the improvement becomes slight when $\text{scale} > 2$.

6. Conclusion

We present Layton, a discrete tokenizer, which leverages the pretrained LDMs assisted by acceleration models for 1024-pixel image reconstruction with only 256 tokens. It is also extended to text-to-image generation models, LaytonGen, through an autoregressive model. Extensive experiments demonstrate our Layton outperforms the existing methods for high-resolution reconstruction. Our LaytonGen shows strong capability to generate high-quality images, achieving 0.73 score on GenEval benchmark.

References

- [1] Huiwen Chang, Han Zhang, Jarred Barber, Aaron Maschinot, Jose Lezama, Lu Jiang, Ming-Hsuan Yang, Kevin Patrick Murphy, William T Freeman, Michael Rubinstein, et al. Muse: Text-to-image generation via masked generative transformers. In *International Conference on Machine Learning*, pages 4055–4075. PMLR, 2023. 2, 3
- [2] Huiwen Chang, Han Zhang, Lu Jiang, Ce Liu, and William T Freeman. Maskgit: Masked generative image transformer. In *2022 IEEE/CVF Conference on Computer Vision and Pattern Recognition (CVPR)*, pages 11305–11315. IEEE, 2022. 2, 3
- [3] Jia Deng, Wei Dong, Richard Socher, Li Jia Li, Kai Li, and Li Fei-Fei. Imagenet: A large-scale hierarchical image database. In *2009 IEEE Conference on Computer Vision and Pattern Recognition, CVPR 2009*, pages 248–255. IEEE Computer Society, 2009. 2, 6
- [4] Ming Ding, Wendi Zheng, Wenyi Hong, and Jie Tang. Cogview2: Faster and better text-to-image generation via hierarchical transformers. In *Advances in Neural Information Processing Systems*, 2022. 2
- [5] Patrick Esser, Sumith Kulal, Andreas Blattmann, Rahim Entezari, Jonas Müller, Harry Saini, Yam Levi, Dominik Lorenz, Axel Sauer, Frederic Boesel, et al. Scaling rectified flow transformers for high-resolution image synthesis. In *International Conference on Machine Learning*, pages 12606–12633. PMLR, 2024. 2, 3, 6, 7, 8
- [6] Patrick Esser, Sumith Kulal, Andreas Blattmann, Rahim Entezari, Jonas Müller, Harry Saini, Yam Levi, Dominik Lorenz, Axel Sauer, Frederic Boesel, et al. Scaling rectified flow transformers for high-resolution image synthesis. In *International Conference on Machine Learning*, pages 12606–12633. PMLR, 2024. 2, 3, 4
- [7] Patrick Esser, Robin Rombach, and Bjorn Ommer. Taming transformers for high-resolution image synthesis. In *Proceedings of the IEEE/CVF Conference on Computer Vision and Pattern Recognition*, pages 12873–12883, 2021. 2, 3, 7
- [8] Dhruva Ghosh, Hannaneh Hajishirzi, and Ludwig Schmidt. Geneval: An object-focused framework for evaluating text-to-image alignment. *Advances in Neural Information Processing Systems*, 36:52132–52152, 2023. 2, 7
- [9] Martin Heusel, Hubert Ramsauer, Thomas Unterthiner, Bernhard Nessler, and Sepp Hochreiter. Gans trained by a two time-scale update rule converge to a local nash equilibrium. *Advances in neural information processing systems*, 30, 2017. 2, 6
- [10] Jonathan Ho, Ajay Jain, and Pieter Abbeel. Denoising diffusion probabilistic models. *Advances in Neural Information Processing Systems*, 33:6840–6851, 2020. 3
- [11] Jonathan Ho and Tim Salimans. Classifier-free diffusion guidance. *arXiv e-prints*, pages arXiv–2207, 2022. 5
- [12] Yang Jin, Kun Xu, Liwei Chen, Chao Liao, Jianchao Tan, Quzhe Huang, CHEN Bin, Chengru Song, Di ZHANG, Wenwu Ou, et al. Unified language-vision pretraining in llm with dynamic discrete visual tokenization. In *The Twelfth International Conference on Learning Representations*, 2024. 3
- [13] Dongwon Kim, Ju He, Qihang Yu Yu, Chenglin Yang, Xiaohui Shen, Suha Kwak, and Chen Liang-Chieh. Democratizing text-to-image masked generative models with compact text-aware one-dimensional tokens. *arXiv preprint arXiv:2501.07730*, 2025. 2, 3
- [14] Diederik P Kingma. Auto-encoding variational bayes. *arXiv preprint arXiv:1312.6114*, 2013. 2
- [15] Black Forest Labs. Flux.1-dev. <https://github.com/black-forest-labs/flux>, 2024. 2, 3, 6
- [16] Doyup Lee, Chiheon Kim, Saehoon Kim, Minsu Cho, and Wook-Shin Han. Autoregressive image generation using residual quantization. In *2022 IEEE/CVF Conference on Computer Vision and Pattern Recognition (CVPR)*, pages 11513–11522. IEEE Computer Society, 2022. 2, 3
- [17] Doyup Lee, Chiheon Kim, Saehoon Kim, Minsu Cho, and Wook-Shin Han. Draft-and-revise: Effective image generation with contextual rq-transformer. In *Advances in Neural Information Processing Systems*, 2022. 3
- [18] José Lezama, Huiwen Chang, Lu Jiang, and Irfan Essa. Improved masked image generation with token-critic. In *European Conference on Computer Vision*, pages 70–86, 2022. 3
- [19] Jose Lezama, Tim Salimans, Lu Jiang, Huiwen Chang, Jonathan Ho, and Irfan Essa. Discrete predictor-corrector diffusion models for image synthesis. In *The Eleventh International Conference on Learning Representations*, 2022. 3
- [20] Zhenyi Liao, Qingsong Xie, Chen Chen, Haonan Lu, and Zhijie Deng. Facescore: Benchmarking and enhancing face quality in human generation. *arXiv preprint arXiv:2406.17100*, 2024. 7
- [21] Tsung-Yi Lin, Michael Maire, Serge Belongie, James Hays, Pietro Perona, Deva Ramanan, Piotr Dollár, and C Lawrence Zitnick. Microsoft coco: Common objects in context. In *Computer vision—ECCV 2014: 13th European conference, zurich, Switzerland, September 6–12, 2014, proceedings, part v 13*, pages 740–755. Springer, 2014. 2, 6, 7
- [22] Jiasen Lu, Christopher Clark, Rowan Zellers, Roozbeh Motlaghi, and Aniruddha Kembhavi. Unified-io: A unified model for vision, language, and multi-modal tasks. In *The Eleventh International Conference on Learning Representations*, 2023. 3

- [23] Fabian Mentzer, David Minnen, Eirikur Agustsson, and Michael Tschannen. Finite scalar quantization: Vq-vae made simple. In *The Twelfth International Conference on Learning Representations*, 2024. 3
- [24] David Mizrahi, Roman Bachmann, Oguzhan Fatih Kar, Teresa Yeo, Mingfei Gao, Afshin Dehghan, and Amir Zamir. 4m: Massively multimodal masked modeling. In *Thirty-seventh Conference on Neural Information Processing Systems*. 2
- [25] Playgroundai. Mjhg-30k. <https://huggingface.co/datasets/playgroundai/MJHQ-30K>, 2023. 6
- [26] Dustin Podell, Zion English, Kyle Lacey, Andreas Blattmann, Tim Dockhorn, Jonas Müller, Joe Penna, and Robin Rombach. Sdxl: Improving latent diffusion models for high-resolution image synthesis. In *The Twelfth International Conference on Learning Representations*, 2024. 2, 3, 4, 6, 7, 8
- [27] Liao Qu, Huichao Zhang, Yiheng Liu, Xu Wang, Yi Jiang, Yiming Gao, Hu Ye, Daniel K Du, Zehuan Yuan, and Xinglong Wu. Tokenflow: Unified image tokenizer for multimodal understanding and generation. *arXiv preprint arXiv:2412.03069*, 2024. 2, 3
- [28] Yuxi Ren, Xin Xia, Yanzuo Lu, Jiacheng Zhang, Jie Wu, Pan Xie, XING WANG, and Xuefeng Xiao. Hyper-sd: Trajectory segmented consistency model for efficient image synthesis. In *The Thirty-eighth Annual Conference on Neural Information Processing Systems*, 2024. 2, 4
- [29] Robin Rombach, Andreas Blattmann, Dominik Lorenz, Patrick Esser, and Björn Ommer. High-resolution image synthesis with latent diffusion models. In *2022 IEEE/CVF Conference on Computer Vision and Pattern Recognition (CVPR)*, pages 10674–10685. IEEE, 2022. 6, 8
- [30] Robin Rombach, Andreas Blattmann, Dominik Lorenz, Patrick Esser, and Björn Ommer. High-resolution image synthesis with latent diffusion models. In *Proceedings of the IEEE/CVF Conference on Computer Vision and Pattern Recognition (CVPR)*, pages 10684–10695, June 2022. 8
- [31] Christoph Schuhmann, Romain Beaumont, Richard Vencu, Cade Gordon, Ross Wightman, Mehdi Cherti, Theo Coombes, Aarush Katta, Clayton Mullis, Mitchell Wortsman, et al. Laion-5b: An open large-scale dataset for training next generation image-text models. *Advances in Neural Information Processing Systems*, 35:25278–25294, 2022. 6
- [32] Jie Shi, Chenfei Wu, Jian Liang, Xiang Liu, and Nan Duan. Divae: Photorealistic images synthesis with denoising diffusion decoder. *arXiv e-prints*, pages arXiv–2206, 2022. 2, 3
- [33] Peize Sun, Yi Jiang, Shoufa Chen, Shilong Zhang, Bingyue Peng, Ping Luo, and Zehuan Yuan. Autoregressive model beats diffusion: Llama for scalable image generation. *arXiv preprint arXiv:2406.06525*, 2024. 2, 3, 6, 7, 8
- [34] Haotian Tang, Yecheng Wu, Shang Yang, Enze Xie, Junsong Chen, Junyu Chen, Zhuoyang Zhang, Han Cai, Yao Lu, and Song Han. Hart: Efficient visual generation with hybrid autoregressive transformer. In *The Thirteenth International Conference on Learning Representations*, 2024. 2
- [35] Haotian Tang, Yecheng Wu, Shang Yang, Enze Xie, Junsong Chen, Junyu Chen, Zhuoyang Zhang, Han Cai, Yao Lu, and Song Han. Hart: Efficient visual generation with hybrid autoregressive transformer. *arXiv e-prints*, pages arXiv–2410, 2024. 6, 8
- [36] Chameleon Team. Chameleon: Mixed-modal early-fusion foundation models. *arXiv e-prints*, pages arXiv–2405, 2024. 3
- [37] Keyu Tian, Yi Jiang, Zehuan Yuan, BINGYUE PENG, and Liwei Wang. Visual autoregressive modeling: Scalable image generation via next-scale prediction. In *The Thirty-eighth Annual Conference on Neural Information Processing Systems*, 2024. 2
- [38] Aaron Van Den Oord, Oriol Vinyals, et al. Neural discrete representation learning. *Adv. Neural Inform. Process. Syst.*, 30, 2017. 2, 3
- [39] Peng Wang, Shuai Bai, Sinan Tan, Shijie Wang, Zhihao Fan, Jinze Bai, Keqin Chen, Xuejing Liu, Jialin Wang, Wenbin Ge, et al. Qwen2-vl: Enhancing vision-language model’s perception of the world at any resolution. *arXiv e-prints*, pages arXiv–2409, 2024. 6
- [40] Xinlong Wang, Xiaosong Zhang, Zhengxiong Luo, Quan Sun, Yufeng Cui, Jinsheng Wang, Fan Zhang, Yuezhe Wang, Zhen Li, Qiyang Yu, et al. Emu3: Next-token prediction is all you need. *arXiv e-prints*, pages arXiv–2409, 2024. 2
- [41] Xiaoshi Wu, Yiming Hao, Keqiang Sun, Yixiong Chen, Feng Zhu, Rui Zhao, and Hongsheng Li. Human preference score v2: A solid benchmark for evaluating human preferences of text-to-image synthesis. *arXiv e-prints*, pages arXiv–2306, 2023. 7
- [42] Yecheng Wu, Zhuoyang Zhang, Junyu Chen, Haotian Tang, Dacheng Li, Yunhao Fang, Ligeng Zhu, Enze Xie, Hongxu Yin, Li Yi, et al. Vila-u: a unified foundation model integrating visual understanding and generation. *arXiv e-prints*, pages arXiv–2409, 2024. 3
- [43] Jinheng Xie, Weijia Mao, Zechen Bai, David Junhao Zhang, Weihao Wang, Kevin Qinghong Lin, Yuchao Gu, Zhijie Chen, Zhenheng Yang, and Mike Zheng Shou. Show-o: One single transformer to unify multimodal understanding and generation. *arXiv e-prints*, pages arXiv–2408, 2024. 2, 6, 8
- [44] Qingsong Xie, Zhenyi Liao, Zhijie Deng, Haonan Lu, et al. Tlcm: Training-efficient latent consistency model for image generation with 2-8 steps. *arXiv preprint arXiv:2406.05768*, 2024. 2, 4
- [45] Jiazheng Xu, Xiao Liu, Yuchen Wu, Yuxuan Tong, Qinkai Li, Ming Ding, Jie Tang, and Yuxiao Dong. Imagereward: Learning and evaluating human preferences for text-to-image generation. In *Thirty-seventh Conference on Neural Information Processing Systems*, 2023. 6
- [46] Jiahui Yu, Xin Li, Jing Yu Koh, Han Zhang, Ruoming Pang, James Qin, Alexander Ku, Yuanzhong Xu, Jason Baldridge, and Yonghui Wu. Vector-quantized image modeling with improved vqgan. In *International Conference on Learning Representations*, 2022. 2, 3
- [47] Lijun Yu, Jose Lezama, Nitesh Bharadwaj Gundavarapu, Luca Versari, Kihyuk Sohn, David Minnen, Yong Cheng, Agrim Gupta, Xiuye Gu, Alexander G Hauptmann, et al. Language model beats diffusion-tokenizer is key to visual

- generation. In *The Twelfth International Conference on Learning Representations*, 2024. [3](#)
- [48] Qihang Yu, Mark Weber, Xueqing Deng, Xiaohui Shen, Daniel Cremers, and Liang-Chieh Chen. An image is worth 32 tokens for reconstruction and generation. In *The Thirty-eighth Annual Conference on Neural Information Processing Systems*, 2024. [2](#), [3](#), [6](#), [7](#)
- [49] Jun Zhan, Junqi Dai, Jiasheng Ye, Yunhua Zhou, Dong Zhang, Zhigeng Liu, Xin Zhang, Ruibin Yuan, Ge Zhang, Linyang Li, et al. Anygpt: Unified multimodal llm with discrete sequence modeling. In *Proceedings of the 62nd Annual Meeting of the Association for Computational Linguistics (Volume 1: Long Papers)*, pages 9637–9662, 2024. [3](#)
- [50] Lvmin Zhang, Anyi Rao, and Maneesh Agrawala. Adding conditional control to text-to-image diffusion models. In *2023 IEEE/CVF International Conference on Computer Vision (ICCV)*, pages 3813–3824. IEEE Computer Society, 2023. [2](#), [4](#)
- [51] Richard Yi Zhang, Phillip Isola, Alexei A Efros, Eli Shechtman, and Oliver Wang. The unreasonable effectiveness of deep features as a perceptual metric. In *31st Meeting of the IEEE/CVF Conference on Computer Vision and Pattern Recognition, CVPR 2018*, pages 586–595. IEEE Computer Society, 2018. [5](#), [6](#)
- [52] Sixian Zhang, Bohan Wang, Junqiang Wu, Yan Li, Tingting Gao, Di Zhang, and Zhongyuan Wang. Learning multi-dimensional human preference for text-to-image generation. In *2024 IEEE/CVF Conference on Computer Vision and Pattern Recognition (CVPR)*, pages 8018–8027. IEEE Computer Society, 2024. [6](#)
- [53] Yue Zhao, Yuanjun Xiong, and Philipp Krähenbühl. Image and video tokenization with binary spherical quantization. *arXiv e-prints*, pages arXiv–2406, 2024. [3](#)

Layton: Latent Consistency Tokenizer for 1024-pixel Image Reconstruction and Generation by 256 Tokens

Supplementary Material

7. Implementation Details

We adopt the same encoder structure in LlamaGen and SDXL as the pre-trained LDM. For tokenizer training, diffusion loss is first used to train Layton for 80000 iterations, and then reconstruction loss is exploited to further optimize Layton for 30000 iterations. 4 A100 is used with Adam Optimizer to train Layton, where $\beta_1 = 0.9$, $\beta_2 = 0.99$, learning rate (lr) = $1e-5$, total batch size = 4. All the images x_0 with progressive resolution from 512 to 1024 pixel size are encoded into latent space by SDXL-VAE. The images are also randomly resized to $\{224, 256, 288\}$ pixel size, feeding into encoder and quantizer, yielding condition of LDM. During the training stage of LaytonGen, flan-t5-xl is utilized to extract text features, GPT-XL architecture with 675M parameters in LlamaGen is used as AR model. In this stage, we set lr= $1e-4$, batch size=320 with 8 A100. AdamW optimizer with $\beta_1 = 0.9$, $\beta_2 = 0.99$ is used to train LaytonGen for 200K iterations. All the tokenizers are trained on ImageNet, except for those specifically marked with an asterisk (*), which are trained on synthetic data.

8. Qualitative Visualization Results

We present extended comparative results for image reconstruction in Fig. 5 and additional text-conditioned image generation outcomes in Fig. 6.

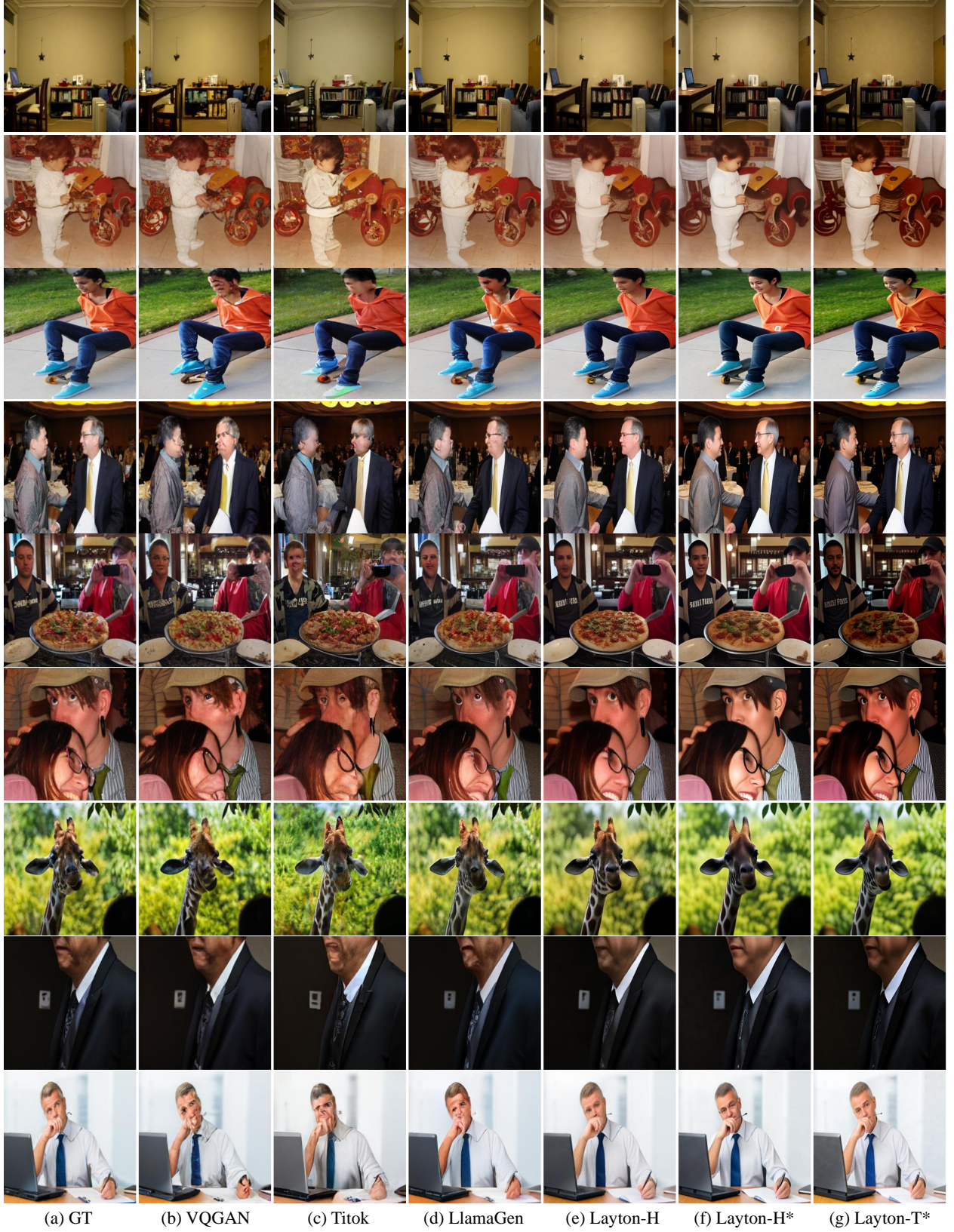
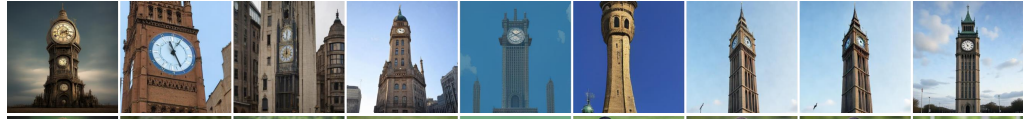
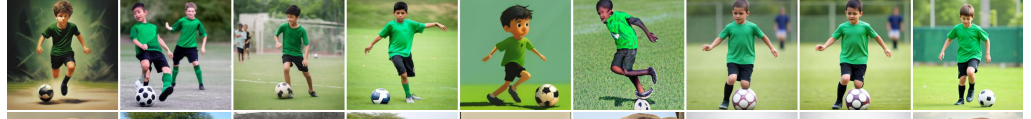


Figure 5: More examples on visual comparisons of images reconstruction with different methods. From left to right, ground truth, VQGAN, TiTok, LLamaGen, Layton-H, Layton-H* and Layton-T*.

A large tower that has a big clock at top



A boy with a green shirt and a black pair of shorts playing soccer



A man standing next to an elephant next to his trunk



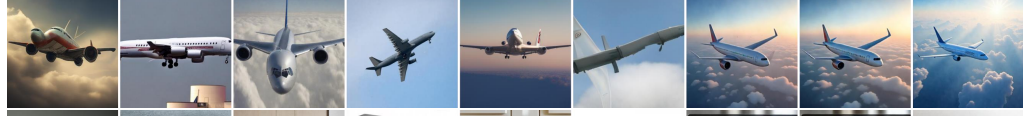
A photo of three computer keyboards



A man in a hat leaning against a pole



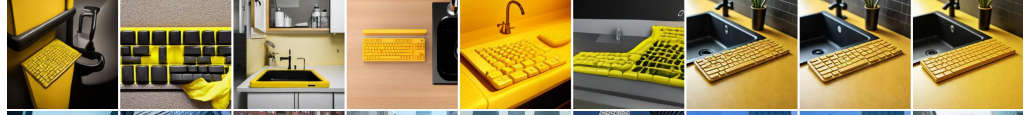
A large air plane flying thru the air



A microwave oven with a tray on the bottom



A photo of a yellow computer keyboard and a black sink



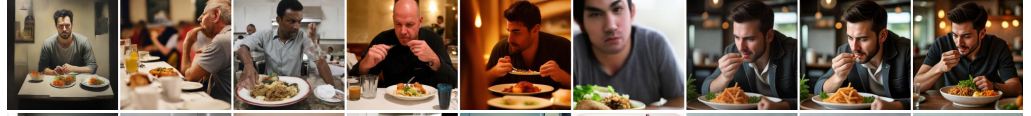
A red fire hydrant in front of a skyscraper



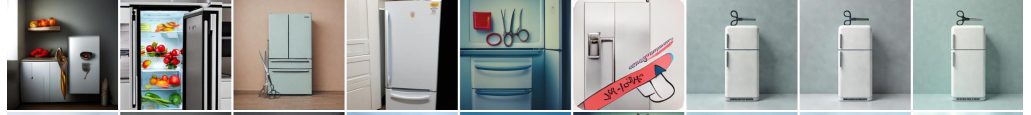
A female is talking on the phone and a laptop on a table



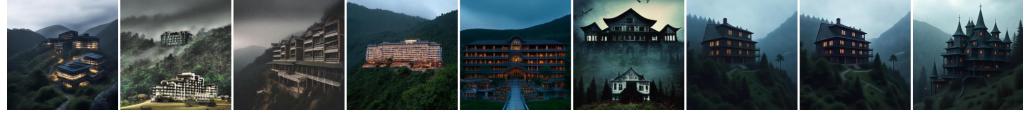
A man looks on as he finishes his meal



a photo of a refrigerator below a scissors



a spooky looking hotel resort in the hills



(a) (b) (c) (d) (e) (f) (g) (h) (i)

Figure 6: More examples on text-conditioned generation of different methods. From left to right, (a)HART, (b)SD1.5, (c)SDXL, (d)SD3, (e)Show-o, (f)LlamaGen, (g)LaytonGen-H, (h)LaytonGen-H* and (i)LaytonGen-T*.